Zitierweise: *Angew. Chem. Int. Ed.* **2024**, *63*, e202316915
doi.org/10.1002/anie.202316915

Carbon Nanodots | Hot Paper

Synthetic Strategies for the Selective Functionalization of Carbon Nanodots Allow Optically Communicating Suprastructures

Beatrice Bartolomei, Maria Sbacchi, Cristian Rosso, Ayse Günay-Gürer, Lukáš Zdražil, Alejandro Cadranel, Slavko Kralj, Dirk M. Guldi, and Maurizio Prato**

Abstract: The surface of Carbon Nanodots (CNDs) stands as a rich chemical platform, able to regulate the interactions between particles and external species. Performing selective functionalization of these nanoscale entities is of practical importance, however, it still represents a considerable challenge. In this work, we exploited the organic chemistry toolbox to install target functionalities on the CND surface, while monitoring the chemical changes on the material's outer shell through nuclear magnetic resonance spectroscopy. Following this, we investigated the use of click chemistry to covalently connect CNDs of different nature *en-route* towards covalent suprastructures with unprecedent molecular control. The different photophysical properties of the connected particles allowed their optical communication in the excited state. This work paves the way for the development of selective and addressable CND building blocks which can act as modular nanoscale synthons that mirror the long-established reactivity of molecular organic synthesis.

Introduction

In recent years, the focus of nanoscience and nanotechnology is gradually shifting from the synthesis of individual components to their assembly into larger systems and materials. Indeed, the precise organization of matter across multiple length scales is of particular interest because of its great potential for advanced functions and properties.[1,2] The key challenges for the bottom-up assembly of nanoarchitectures relate to the control of surface composition of the building blocks. Specifically, exerting a precise control on the chemical functionalities of nanoparticles enables to guide their selective reaction towards the synthesis of complex suprastructures.[3] This approach is similar to the total chemical synthesis of complicated natural products from small organic molecules.[4]

In this context, Carbon Nanodots (CNDs), nanosized photoluminescent carbon particles, represent smart starting units. Indeed, CNDs are generally described as composed of a carbon-based core covered by surface functionalities.[5,6] The superficial properties regulate the interaction of the particles with the surrounding environment in terms of recognition and binding, reactivity, solvation, as well as the

[*] B. Bartolomei, M. Sbacchi, Dr. C. Rosso, Prof. M. Prato
Department of Chemical and Pharmaceutical Sciences, INSTM UdR Trieste, University of Trieste
via Licio Giorgieri 1, 34127 Trieste (Italy)
E-mail: prato@units.it

Dr. C. Rosso
Current address: Department of Chemical Sciences, University of Padova
via Marzolo 1, 35131 Padova (Italy)

A. Günay-Gürer, Dr. L. Zdražil, Dr. A. Cadranel, Prof. D. M. Guldi
Department of Chemistry and Pharmacy, Interdisciplinary Center for Molecular Materials (ICMM), Friedrich-Alexander-Universität Erlangen-Nürnberg
91058 Erlangen (Germany)
E-mail: dirk.guldi@fau.de

Dr. L. Zdražil
Regional Centre of Advanced Technologies and Materials, Czech Advanced Technology and Research Institute (CATRIN), Palacký University Olomouc
Šlechtitelů 241/27, 78371 Olomouc (Czech Republic)

Dr. A. Cadranel
Departamento de Química Inorgánica, Analítica y Química Física, Facultad de Ciencias Exactas y Naturales, Universidad de Buenos Aires
C1428EHA Buenos Aires (Argentina)
and
CONICET—Universidad de Buenos Aires, Instituto de Química Física de Materiales, Medio Ambiente y Energía, (INQUIMAE)
C1428EHA Buenos Aires (Argentina)

Dr. S. Kralj
Materials Synthesis Department, Jožef Stefan Institute
Jamova cesta 39, 1000 Ljubljana (Slovenia)
and
Department of Pharmaceutical Technology, Faculty of Pharmacy, University of Ljubljana
Aškerčeva 7, 1000 Ljubljana (Slovenia)

Prof. M. Prato
Centre for Cooperative Research in Biomaterials (CIC BiomaGUNE), Basque Research and Technology Alliance (BRTA)
Paseo de Miramón 194, 20014 Donostia San Sebastián (Spain)
and
Basque Fdn Sci, Ikerbasque
48013 Bilbao (Spain)

material processibility. For example, the surface groups on CNDs were widely explored to establish non-covalent bonds, such as electrostatic interactions, coordinative bonds, and hydrogen bonds with various other molecules and materials.[7–9] Otherwise, covalent derivatization has been exploited to finely modify the particle surface, anchoring the desired species to the CNDs.[10] The so-developed functional materials have as ultimate goal the preparation of valuable nanohybrids in which the merging of the intrinsic traits of the coupled constituents paves the way to advanced applications within the fields of optoelectronics, photovoltaics, medicinal chemistry, among others.[7,11–16]

To this aim, exerting chemical and constitutional control over the CND coupling with functional species is of paramount importance but it is still challenging. A possible solution to overcome this limitation might be the application of the molecular synthetic toolbox into the nanoscale level. In this regard, click chemistry stands as a prominent strategy, enabling the selective, easy and direct linking of nanoparticles with target species. The click methodology allows to achieve a universal connection of chemical entities, avoiding the use of highly reactive or cross-reactive intermediates.[17] For these reasons, click chemistry has been applied to a myriad of systems, spanning from chemistry to material science, along with biology.[18–21] Specifically, the Cu(I)-catalyzed alkyne-azide cycloaddition (CuAAC) is one of the most studied click transformations for the fast interconnection of tagged species at room temperature.[22]

In this work, we investigated the application of CuAAC reactions to CNDs in order to selectively bind these materials with target molecules. Thereafter, the so-developed general methodology has been extended to connect CNDs of different nature, thus forming unprecedented covalent suprastructures with remarkable molecular control.

In particular, we employed two sets of CNDs previously developed in our group. **CNDs-1** are synthesized starting from *L*-arginine and ethylendiamine, while **CNDs-2** are prepared from citric acid and (*S*)-2-(aminomethyl)-1-Boc-pyrrolidine (Figure 1).[23,24] These particles present emission in different regions of the visible spectrum, while they possess amines and other polar functionalities on the surface, which allow their post-functionalization through coupling reactions with acyl chlorides. Initially, we used a terminal fluorinated tag to quantify the number of anchoring points on the CND surface and, based on these data, we moved to the installation of alkyne and azide moieties on the materials. Finally, a click reaction between the two complementary building blocks afforded the covalent hybrids, in a selective fashion. This allowed us to build optical communicating suprastructures that might lay the foundations towards the design of advanced interactive architectures.

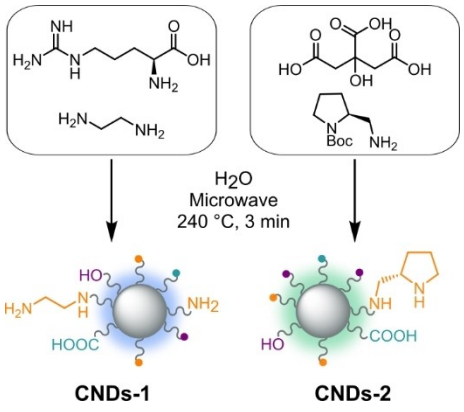

Figure 1. General Scheme for the synthesis of **CNDs-1** and **CNDs-2** reported in ref. [23–24]. The colored labels correspond to the depicted functionalities.

Results and Discussion

Assessment of the reactive CND functionalities

CNDs-1 and **CNDs-2** present numerous surface functionalities such as amines, alcohols, carboxylic acids, among others. Based on this, a general reactivity for their functionalization relies on the coupling reaction with acyl chlorides. To exert a control on the nanoparticle derivatization, it is pivotal to reveal the number of installed moieties on the material surface after the functionalization reaction. To this aim, we implemented a fluorine-labeling strategy combined with ^{19}F NMR. Indeed, this technique is a sensitive tool to investigate the chemistry of the outer shell of CNDs without interference from the other signals of the nanoparticles.[25,26]

In this regard, the molecular probe 12,12,12-trifluorododec-10-ynoic acid (**1**) has been synthesized and subsequently converted into the corresponding acyl chloride **2**. The coupling reaction between **2** and **CNDs-1** was carried out in *N*,*N*-dimethylformamide (DMF) in the presence of triethylamine (TEA) as a base, at room temperature (Figure 2a). The obtained functionalized nanoparticles resulted to be soluble in organic solvents, such as chloroform. Based on this, the purification of these materials was performed with a chloroform/water extraction, to remove the coupling by-products, followed by a precipitation with diethyl ether to get rid of the unreacted **2**. The so-obtained **CNDs-3** were characterized through ^{1}H NMR, that displayed the diagnostic signals associated to the protons close to the carboxyl group at around 2–2.5 ppm, which are more shielded with respect to those of **2**, in agreement with the presence of a less electron-withdrawing group (Figure 2b–c). Moreover, the peaks associated to the alkyl protons at around 1–1.5 ppm experienced a broadening due to the proximity to the CND surface.[27,28] Additionally, diffusion ordered spectroscopy (DOSY) was employed to further confirm the successful functionalization of **CNDs-1**. As a result, the diffusion coefficient obtained for **1** is 8.05×10^{-6} cm^2 s^{-1} while **CNDs-3** exhibit a value of 2.57×10^{-6} cm^2 s^{-1}. The smaller coefficient obtained for the latter is in agreement with a decrease in the diffusion rate of the molecule when it is attached on CND surface (Figure 2d).[29] Finally, a typical ^{19}F NMR signal was detected in the **CNDs-3** sample at −49 ppm, similar to that presents in the starting material **2** (insets in Figure 2b–c). This specific NMR peak can reveal

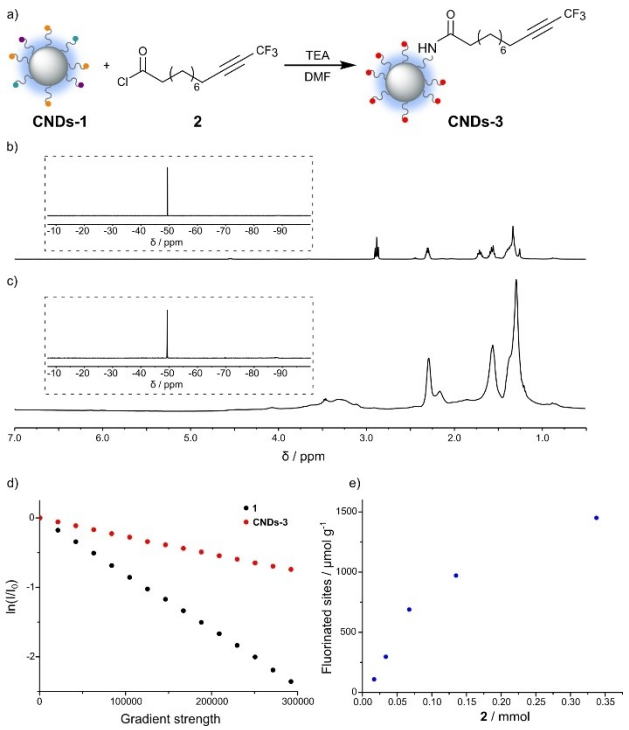

Figure 2. a) General scheme for the coupling between **CNDs-1** and **2**. The colored labels correspond to the depicted functionalities. Conditions: **CNDs-1** (25 mg), **2** (0.34 mmol), TEA (0.34 mmol), DMF (4 mL), 3 d. b) **2**, ^{1}H NMR ($CDCl_3$, 400 MHz, rt), inset ^{19}F NMR ($CDCl_3$, 376 MHz, rt). c) **CNDs-3**, ^{1}H NMR ($CDCl_3$, 400 MHz, rt), inset ^{19}F NMR ($CDCl_3$, 376 MHz, rt). d) DOSY ($CDCl_3$, 500 MHz, rt), normalized logarithmic signal decay of representative peaks (2.3 ppm) of **1** (black) and **CNDs-3** (red) as function of gradient strength. e) Number of fluorinated sites installed on **CNDs-1** after reaction with increasing amounts of **2** (0.02–0.14 mmol) followed by saturation with octanoyl chloride (0.34 mmol) and TEA (0.34 mmol).

the number of fluorinated sites installed on **CNDs-3**, by using an internal standard—namely trifluorotoluene—thus resulting to be 1450 μmol/g is in agreement with previous reports.[23,26] The same protocol was applied to **CNDs-2**, giving the corresponding functionalized product with 320 μmol/g of fluorinated superficial moieties (Figure S5).

Considering **CNDs-1** as a model, we proved the possibility to control the number of fluorinated moieties that we can install on CNDs. Indeed, we repeated the reaction on **CNDs-1** employing lower amounts of **2** and saturating the remaining functionalities with octanoyl chloride to ensure the solubility in organic solvents (Figures S1–S4). The quantification of the corresponding products provided the trend reported in Figure 2e. This outcome demonstrates the possibility of finely tuning the coverage of CNDs surface by simply changing the stoichiometry of the employed reactant.

Click reactions between CNDs and model molecules

With the aim of performing click reactions between carbon-based nanoparticles, we functionalized **CNDs-1** with an acyl chloride bearing a terminal alkyne, namely 11-(prop-2-yn-1-yloxy)undecanoyl chloride (**3**), by employing the previously described conditions (0.34 mmol of **3**, corresponding to the fifth point of trend reported in Figure 2e). The resulting **CNDs-4** show the diagnostic alkyne signal at ^{1}H NMR at around 2.4 ppm, along with the α-oxo protons at 4.1 and 3.5 ppm (Figure 3b and Figure S6). We initially allowed this functionalized material to react with a model fluorinated azide, 1-(azidomethyl)-3,5-bis(trifluoromethyl)benzene (**4**). This click reaction was carried out in a biphasic system ($CHCl_3$:H_2O, 1:1 v/v) using $CuSO_4$ as catalyst and sodium ascorbate (NaAsc) as reducing agent (see Supporting Information for details).[30] The NMR of **CNDs-5** displays the presence of the triazole signal at 7.6 ppm and the absence of the signal related to the terminal alkyne of **CNDs-4**, together with the deshielding of the protons adjacent to the heterocyclic system (Figure 3d). Furthermore, an intense ^{19}F NMR peak at around −63 ppm confirmed the success of the reaction (Figure S13). At the same time, we functionalized **CNDs-2** with an azide moiety using 11-azidoundecanoyl chloride, hence obtaining **CNDs-6**, which present the key ^{1}H NMR signal at around 3.2 ppm related to the protons in alpha to the azide (Figure S9). In addition, the presence of azide functionality was further assessed by the FT-IR which shows the typical peak at about 2100 cm^{-1}, which is absent in **CNDs-2** (Figure S10).[24] In this case, the cycloaddition reaction with a model molecular alkyne, 1-((prop-2-yn-1-yloxy)methyl)-3,5-bis(trifluoromethyl)benzene, provided the corresponding adduct (Figures S14–S15). These results establish a general methodology to functionalize CNDs by click chemistry, leading the way to couple these particles with desired species through high selectivity and control.

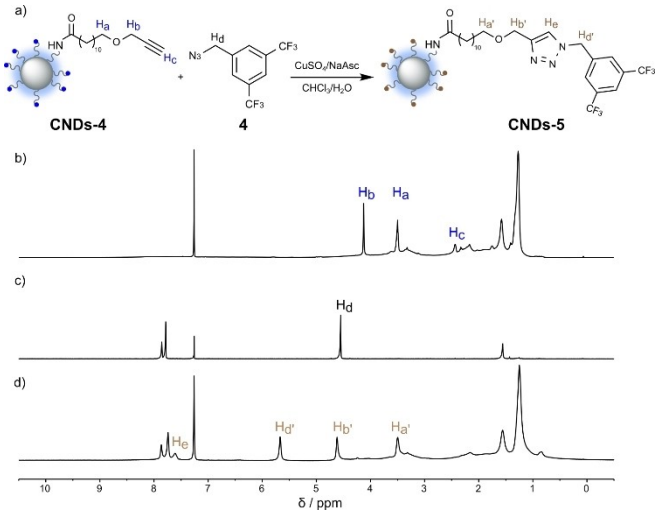

Figure 3. a) General scheme for the click reaction between **CNDs-4** and **4**. The colored labels correspond to the depicted functionalities. Conditions: **CNDs-4** (15 mg), **4** (0.2 mmol), $CuSO_4 \cdot 5H_2O$ (0.02 mmol), NaAsc (0.04 mmol), $CHCl_3$ (1 mL), H_2O (1 mL), 24 h. b–d) ^{1}H NMR ($CDCl_3$, 400 MHz, rt) of **CNDs-4**, **4**, **CNDs-5**.

Click reactions between CNDs

In a next step, we prepared interconnected CND suprastructures by performing a click reaction between the two complementary building blocks **CNDs-4** and **CNDs-6**. Remarkably, the previously performed quantifications allowed us to exactly select the reaction stoichiometry. In particular, the alkyne-bearing material was employed in slight excess with respect to the azide counterpart (1.5 equiv.) to ensure a complete formation of the desired product. The final nanomaterial **CNDs-7** was purified through size exclusion chromatography (SEC, see Supporting Information for details). The ^{1}H NMR analysis clearly showed the successful interconnection of two different nanodots through the classical triazole signal at around 7.5 ppm along with the related signals at 4.6 and 4.3 ppm (Figure 4b). Transmission electron microscopy (TEM) of **CNDs-7** shows the presence of larger structures compared to the dimensions of both **CNDs-4** and **CNDs-6** (see Figure 4c–d and Figures S7, S11). Moreover, in Figure 4d, we can clearly observe the presence of single dots inside the suprastructure.

Based on the quantification of the surface functionalities that we previously performed, we can decrease the number of alkyne moieties that we install on **CNDs-1** in order to tune the final structure. Based on this, we prepared **CNDs-8** starting from **CNDs-1** and lower amount of **3** (0.07 mmol, corresponding to the third point of trend reported in Figure 2e, see Supporting Information for details). By means of performing the click reaction between **CNDs-8** and **CNDs-6** we obtained the material **CNDs-9**. Compared to the previous case, TEM images (Figure 4e–f) revealed smaller and less crowded structures, in agreement with a reduced number of reactive functionalities present on **CNDs-8**. This result highlights the possibility to tune the arrangement of the final suprastructures by controlling the number of reactive functionalities installed on the particles.

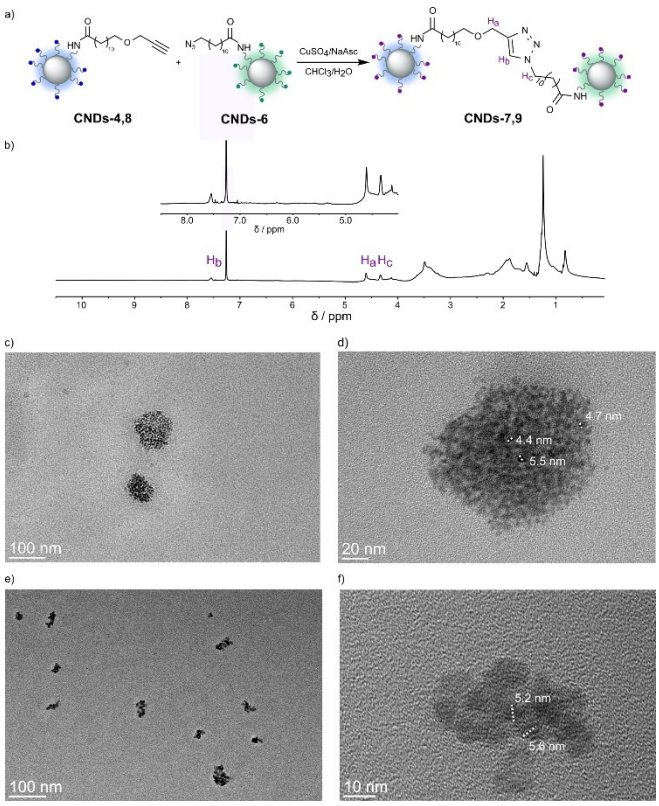

Figure 4. a) General scheme for the click reaction between **CNDs-4,8** and **CNDs-6**. The colored labels correspond to the depicted functionalities. Conditions: **CNDs-4,8** (5–10 mg), **CNDs-6** (15 mg), $CuSO_4 \cdot 5H_2O$ (0.005 mmol), NaAsc (0.01 mmol), $CHCl_3$ (1 mL), H_2O (1 mL), 24 h. b) **CNDs-7**, ^{1}H NMR ($CDCl_3$, 400 MHz, rt). c–d) TEM images of **CNDs-7**. e–f) TEM images of **CNDs-9**.

Photophysical studies on covalent suprastructures

The different photophysical features of the connected CNDs paves the way to study their excited state behavior and interactions. In particular, ground-state electronic properties of **CNDs-9** suprastructures and those of the individual **CNDs-8** and **CNDs-6** fragments were investigated using absorption spectroscopy. **CNDs-8** in DMF shows absorption features in the UV region lacking defined maxima and tailing into the visible region to about 500 nm. **CNDs-6** also shows these broad absorptions, together with a distinct maximum at 335 nm (Figure S20). A feature within the spectral range of 300 to 400 nm is commonly associated with n-π* transitions originating from surface or fluorophore states involving nitrogen-rich groups.[31,32] The 335 nm signature is broadened in **CNDs-9**. We take this broadening as evidence for the presence of the **CNDs-6** fragment in the suprastructures. Moreover, it suggests ground-state electronic interactions between the **CNDs-8** and **CNDs-6** fragments after the click reaction.

To probe the excited-state electronic interactions in the **CNDs-9** suprastructures, photoluminescence (PL) excitation-emission mapping was conducted (Figure 5a–c). PL emission from **CNDs-8**, **CNDs-6**, and **CNDs-9** was found to be excitation-dependent, which usually either points to the intrinsic variability of CNDs within the ensemble or indicates the existence of several emissive states.[23,24,32–35] The PL excitation-emission map of **CNDs-8** in DMF featured a PL emission maximum at around 410 nm when excited at 340 nm (Figure 5a). Conversely, for **CNDs-6**, a significant redshift was observed for both PL excitation and PL emission, with maxima at 365 and 450 nm, respectively (Figure 5b). Moreover, the PL behavior of **CNDs-9** closely resembles that of **CNDs-6** (Figure 5c). Consequently, all of them gave rise to absorption features in the same energy range. But, the PL active states in **CNDs-6** are lower in energy compared to those in **CNDs-8**. In **CNDs-9**, only **CNDs-6**-like low-energy PL emission dominates. This points to an **CNDs-8**-to-**CNDs-6** energy transfer in the **CNDs-9** nanoconjugate. The PL quantum yields (QY) were measured using the absolute method using an integrating sphere following photo-excitation at 350 nm. The PL QYs were 5.0 %, 10.3 %, and 4.9 % for **CNDs-8**, **CNDs-6** and **CNDs-9**, respectively.

Next, we utilized time-resolved emission spectroscopy (TRES) to study the PL emission dynamics of both

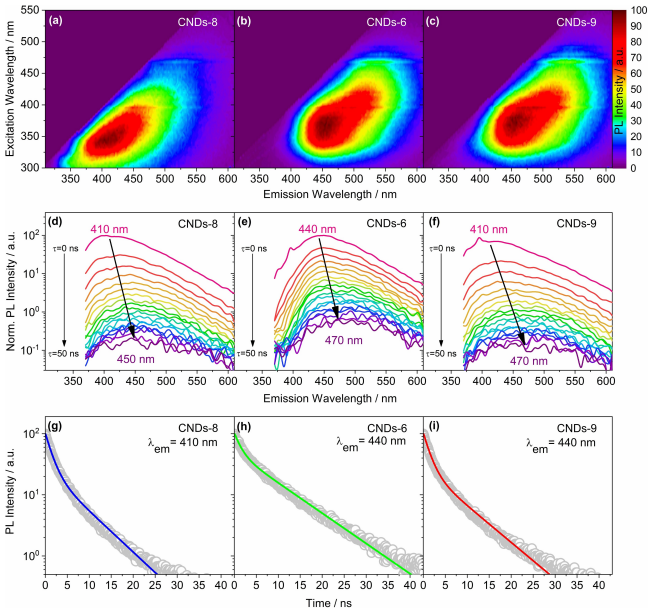

Figure 5. Steady-state and time-resolved PL of **CNDs-8**, **CNDs-6**, and **CNDs-9** in DMF. a)–c) Excitation-emission color maps of **CNDs-8**, **CNDs-6**, and **CNDs-9**. d)–f) Time-resolved emission spectra of **CNDs-8**, **CNDs-6**, and **CNDs-9** measured under the same conditions as in the steady-state experiments under 355 nm excitation. g)–i) Biexponential fitting of TRES data at different wavelengths resulting from global analysis (PL decays were collected at individual PL emission maxima).

individual **CNDs-8** and **CNDs-6** next to that of **CNDs-9** nanoconjugate on the nanosecond timescale (Figure 5d–f and Figure S21). Upon 355 nm excitation, **CNDs-8** and **CNDs-6** both displayed spectral shifts over time, that is, from 410 to 450 nm and from 440 to 470 nm, respectively (Figure 5d–e). More importantly, **CNDs-9** showed the most pronounced spectral transition from 410 to 470 nm in the emission spectrum, supporting our initial hypothesis of energy transfer from high-energy-emitting **CNDs-8** to low-energy-emitting **CNDs-6**. As the presence of excitation-dependent emission reflects the intricate nature of the CNDs PL, a biexponential fitting was necessary (Figure 5g–i).[35] Global analysis of the data afforded emission lifetimes of 2.0 and 8.0 ns for **CNDs-8**, 2.4 and 9.9 ns for **CNDs-6**, and 1.4 and 7.1 ns for **CNDs-9**. The fact that **CNDs-9** reveals the shortest lifetimes prompts to additional decay channels upon formation of the **CNDs-9** suprastructures and sizeable excited-state electronic interactions. Specifically, the rate constant corresponding to the 2.0 ns component of **CNDs-8** is $5.0\times10^8\ s^{-1}$ and increases to $6.9\times10^8\ s^{-1}$ in **CNDs-9** suprastructures. As such, we ascribe the respective difference to the energy transfer in **CNDs-9** with an underlying rate constant of $1.9\times10^8\ s^{-1}$.

Picosecond excited-state dynamics were studied using femtosecond transient absorption spectroscopy (fsTAS) with 390 nm excitation. **CNDs-8**, **CNDs-6**, and **CNDs-9** yielded similar differential spectra, that is, excited state absorption (ESA) across the entire visible range next to ground state bleaching (GSB) and stimulated emission (SE) around 400 nm. Global analysis of the data was performed based on three exponential functions in each case (Figures S22–S24). Two of them correspond to those nanosecond processes seen in the TRES measurements. Therefore, their lifetimes were fixed during the Global analysis. The remaining lifetime was 60, 49, and 23 ps for **CNDs-8**, **CNDs-6**, and **CNDs-9**, respectively. The differential spectra associated with these picosecond lifetimes are similar for **CNDs-8** and **CNDs-9**, with ESAs above 410 nm (red spectra in Figures S22, S24, S25). **CNDs-6** shows ESAs that maximize at 440 and 575 nm. This indicates that the initially populated excited state in the **CNDs-9** nanoconjugate is centered on the **CNDs-8** fragment. The underlying decay rate constant in the **CNDs-9** is $4.4\times10^{10}\ s^{-1}$, larger than the $1.7\times10^{10}\ s^{-1}$ seen in **CNDs-8**. This indicates an additional reactive channel, i.e. an energy transfer from high-energy **CNDs-8**-centered excited states to low-energy **CNDs-6**-centered excited states, with a rate constant of $2.7\times10^{10}\ s^{-1}$.

Figure 6 summarizes in a Jablonski diagram the excited state processes in **CNDs-8** and **CNDs-6**, as well as in **CNDs-9**. Energy transfer on different timescales in the **CNDs-9** suprastructures stems from two different energy transfer-active configurations, arising from the flexible nature of the linker. On one hand, a proximal configuration between the energy donating **CNDs-8** and the energy accepting **CNDs-6** results in an energy transfer in the picosecond regime, like that seen in electron donor-acceptor systems featuring short linkers.[36,37] On the other hand, a distal separation slows down the energy transfer into the nanosecond regime. This is a common feature in the long-range or bimolecular electron donor-acceptor reactivity.[38–40] It is not possible to rule out the population of additional emissive or non-emissive excited-states in **CNDs-8**, **CNDs-6**, and **CNDs-9**. But our model captures the essential characteristics of their

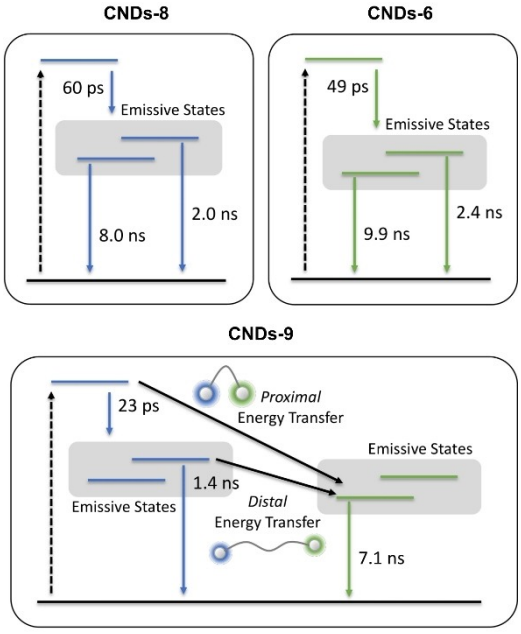

Figure 6. Jablonski diagrams for **CNDs-8**, **CNDs-6**, and **CNDs-9** showing energy transfers in proximal and distal conformations.

photophysics. In fact, TRES and TAS fittings improve only marginally upon consideration of more sophisticated models including additional decay channels.

Conclusion

The ability to assemble nanoscopic components into larger structures and materials depends crucially on the ability to understand in quantitative detail and subsequently engineer the material surfaces. In this work, we investigated CNDs as new versatile building blocks, due to their unique features which stand in between the molecular and the nanoscale realms. We initially quantified the reactive surface functionalities using a fluorine-labeling strategy combined with ^{19}F NMR spectroscopy. Subsequently, we exploited click chemistry to selectively bind CNDs with target probe molecules. Thereafter, the so-developed general methodology has been extended to interconnect CNDs of different nature, thus forming unprecedented covalent suprastructures with remarkable molecular control. The different photophysical features of the connected CNDs set the stage to study their excited state properties and interactions. Specifically, photophysical studies on alkyne- and azide-functionalized CNDs revealed peculiar UV/Visible absorptions and excitation-dependent emissions. Their covalently-linked suprastructures showed optical communication between the different types of particles. Hence, high-energy-emitting alkyne-particles turned out to be engaged in energy transfer processes towards low-energy-emitting azide-particle acceptors. This phenomenon is active through two different reaction channels with different timescales, depending on the conformation of the bridge.

Our contribution aims to establish a new branch in the CND field triggering the development of novel covalent assemblies based on carbon particles. For example, the possibility of controlling the concentration of reacting functionalities installed on CNDs can be used to design nanoscale architectures characterized by peculiar shapes and properties.[41,42] Also, the proposed methodology can allow the production of porous CND-networks which can find applications in a variety of fields, spanning from catalysis to waste-water treatment.[43–45]

Acknowledgements

M. P. is the AXA Chair for Bionanotechnology (2016–2026). The authors gratefully acknowledge the financial support from the European Research Council (ERC AdG-2019 n.885323, e-DOTS), the Spanish Ministry of Economy and Competitiveness MINECO (project PID2019-108523RBI00), the University of Trieste, INSTM, the Italian Ministry of Education MIUR (cofin Prot. 2017PBXPN4) and the Maria de Maeztu Units of Excellence Program from the Spanish State Research Agency (Grant No. MDM-2017-0720). The authors gratefully acknowledge the funding by the "Solar Energy goes Hybrid" Initiative of the Bavarian Ministry for Science, Culture, and Education (SolTech) and the Deutsche Forschungsgemeinschaft (DFG) via SFB 953 "Synthetic Carbon Allotropes". A. C. is an ALN associate and a member of CIC–CONICET. This research was also funded by the Slovenian Research Agency (ARIS) through the core funding No. P2 0089 and ARIS projects No. J2-3043, J2-3040, J2-3046, J3-3079, and J7-4420. The authors also acknowledge the CENN Nanocenter (Slovenia) for TEM access.

Conflict of Interest

The authors declare no conflict of interest.

Data Availability Statement

The data that support the findings of this study are available in the supplementary material of this article.

Keywords: Carbon Nanodots · Click Chemistry · Nanotechnology · Particle Network · Self-Assembly

[1] K. J. M. Bishop, C. E. Wilmer, S. Soh, B. A. Grzybowski, *Small* **2009**, *5*, 1600–1630.
[2] M. Liu, M. Yang, X. Wan, Z. Tang, L. Jiang, S. Wang, *Adv. Mater.* **2023**, *35*, 2208995.
[3] Q. Huo, J. G. Worden, *J. Nanopart. Res.* **2007**, *9*, 1013–1025.
[4] P. S. Baran, *J. Am. Chem. Soc.* **2018**, *140*, 4751–4755.
[5] L. Đorđević, F. Arcudi, M. Cacioppo, M. Prato, *Nat. Nanotechnol.* **2022**, *17*, 112–130.
[6] R. de Boëver, J. R. Town, X. Li, J. P. Claverie, *Chem. Eur. J.* **2022**, *28*, e202200748.
[7] A. Cadranel, V. Strauss, J. T. Margraf, K. A. Winterfeld, C. Vogl, L. Dordević, F. Arcudi, H. Hoelzel, N. Jux, M. Prato, D. M. Guldi, *J. Am. Chem. Soc.* **2018**, *140*, 904–907.
[8] T. Scharl, A. Cadranel, P. Haines, V. Strauss, S. Bernhardt, S. Vela, C. Atienza, F. Gröhn, N. Martín, D. M. Guldi, *Chem. Commun.* **2018**, *54*, 11642–11644.
[9] F. Arcudi, L. Đorđević, *Small* **2023**, *19*, 2300906.
[10] D. Li, Y. Qu, X. Zhang, W. Zheng, A. L. Rogach, S. Qu, *Chem. Eng. J.* **2023**, *454*, 140069.
[11] I. J. Gomez, B. Arnaiz, M. Cacioppo, F. Arcudi, M. Prato, *J. Mater. Chem. B* **2018**, *6*, 5540–5548.
[12] A. Ferrer-Ruiz, T. Scharl, L. Rodríguez-Pérez, A. Cadranel, M. Á. Herranz, N. Martín, D. M. Guldi, *J. Am. Chem. Soc.* **2020**, *142*, 20324–20328.
[13] X. Y. Du, C. F. Wang, G. Wu, S. Chen, *Angew. Chem. Int. Ed.* **2021**, *60*, 8585–8595.
[14] V. M. Badiani, C. Casadevall, M. Miller, S. J. Cobb, R. R. Manuel, I. A. C. Pereira, E. Reisner, *J. Am. Chem. Soc.* **2022**, *144*, 14207–14216.
[15] X. Bu, H. Wang, F. Zhang, Q. Li, J. Zhu, J. Ding, J. Sun, Y. Liu, T. Jiang, *ACS Appl. Nano Mater.* **2022**, *5*, 11447–11457.
[16] Q. He, Z. Wu, J. Li, R. Li, L. Zhang, Y. Liu, *J. Mater. Chem. B* **2023**, *11*, 5094–5100.
[17] H. C. Kolb, M. G. Finn, K. B. Sharpless, *Angew. Chem. Int. Ed.* **2001**, *40*, 2004–2021.
[18] L. Liang, D. Astruc, *Coord. Chem. Rev.* **2011**, *255*, 2933–2945.
[19] M. Meldal, F. Diness, *Trends Chem.* **2020**, *2*, 569–584.

[20] A. K. Agrahari, P. Bose, M. K. Jaiswal, S. Rajkhowa, A. S. Singh, S. Hotha, N. Mishra, V. K. Tiwari, *Chem. Rev.* **2021**, *121*, 7638–7956.
[21] K. F. Suazo, K. Park, M. D. Distefano, *Chem. Rev.* **2021**, *121*, 7178–7248.
[22] V. V. Rostovtsev, L. G. Green, V. V. Fokin, K. B. Sharpless, *Angew. Chem. Int. Ed.* **2002**, *41*, 2596–2599.
[23] F. Arcudi, L. Đorđević, M. Prato, *Angew. Chem. Int. Ed.* **2016**, *55*, 2107–2112.
[24] B. Bartolomei, V. Corti, M. Prato, *Angew. Chem. Int. Ed.* **2023**, *62*, e202305460.
[25] E. N. G. Marsh, Y. Suzuki, *ACS Chem. Biol.* **2014**, *9*, 1242–1250.
[26] G. Filippini, F. Amato, C. Rosso, G. Ragazzon, A. Vega-Peñaloza, X. Companyó, L. Dell'Amico, M. Bonchio, M. Prato, *Chem* **2020**, *6*, 3022–3037.
[27] B. Bartolomei, M. Prato, *Small* **2023**, *19*, 2206714.
[28] B. Bartolomei, A. Bogo, F. Amato, G. Ragazzon, M. Prato, *Angew. Chem. Int. Ed.* **2022**, *61*, e202200038.
[29] P. Groves, *Polym. Chem.* **2017**, *8*, 6700–6708.
[30] F. Himo, T. Lovell, R. Hilgraf, V. V. Rostovtsev, L. Noodleman, K. B. Sharpless, V. V. Fokin, *J. Am. Chem. Soc.* **2005**, *127*, 210–216.
[31] Y. Xiong, J. Schneider, E. V. Ushakova, A. L. Rogach, *Nano Today* **2018**, *23*, 124–139.
[32] G. Ragazzon, A. Cadranel, E. V. Ushakova, Y. Wang, D. M. Guldi, A. L. Rogach, N. A. Kotov, M. Prato, *Chem* **2021**, *7*, 606–628.
[33] S. Khan, A. Gupta, N. C. Verma, C. K. Nandi, *Nano Lett.* **2015**, *15*, 8300–8305.
[34] A. Sharma, T. Gadly, A. Gupta, A. Ballal, S. K. Ghosh, M. Kumbhakar, *J. Phys. Chem. Lett.* **2016**, *7*, 3695–3702.
[35] B. Zhang, B. Wang, E. V. Ushakova, B. He, G. Xing, Z. Tang, A. L. Rogach, S. Qu, *Small* **2023**, *19*, 2204158.
[36] A. Cadranel, P. S. Oviedo, P. Alborés, L. M. Baraldo, D. M. Guldi, J. H. Hodak, *Inorg. Chem.* **2018**, *57*, 3042–3053.
[37] D. Wang, O. C. Fiebig, D. Harris, H. Toporik, Y. Ji, C. Chuang, M. Nairat, A. L. Tong, J. I. Ogren, S. M. Hart, J. Cao, J. N. Sturgis, Y. Mazor, G. S. Schlau-Cohen, *Proc. Natl. Acad. Sci. USA* **2023**, *120*, e2220477120.
[38] G. D. Scholes, *Annu. Rev. Phys. Chem.* **2003**, *54*, 57–87.
[39] A. T. Haedler, K. Kreger, A. Issac, B. Wittmann, M. Kivala, N. Hammer, J. Köhler, H. W. Schmidt, R. Hildner, *Nature* **2015**, *523*, 196–199.
[40] Y. Liu, Y. Ma, Y. Zhao, X. Sun, F. Gándara, H. Furukawa, Z. Liu, H. Zhu, C. Zhu, K. Suenaga, P. Oleynikov, A. S. Alshammari, X. Zhang, O. Terasaki, O. M. Yaghi, *Science* **2016**, *351*, 365–369.
[41] F. Sander, U. Fluch, J. P. Hermes, M. Mayor, *Small* **2014**, *10*, 349–359.
[42] Z. Lin, Y. Xiong, S. Xiang, O. Gang, *J. Am. Chem. Soc.* **2019**, *141*, 6797–6801.
[43] T. Muller, S. Bräse, *Angew. Chem. Int. Ed.* **2011**, *50*, 11844–11845.
[44] Y. Zhang, S. N. Riduan, *Chem. Soc. Rev.* **2012**, *41*, 2083–2094.
[45] Y. Song, J. Phipps, C. Zhu, S. Ma, *Angew. Chem. Int. Ed.* **2023**, *62*, e202216724.

Manuscript received: November 7, 2023
Accepted manuscript online: December 7, 2023
Version of record online: December 27, 2023